Journal of The Electrochemical Society, **164** (7) A1-A9 (2017)
0013-4651/2017/164(7)/A1/9/$37.00 © The Electrochemical Society

Optimal Charging of Li-Ion Batteries via a Single Particle Model with Electrolyte and Thermal Dynamics

H. E. Perez,[a,z] S. Dey,[a] X. Hu,[b] and S. J. Moura[a]

[a]*Energy, Controls, and Applications Lab, Department of Civil and Environmental Engineering, University of California, Berkeley, California 94720, USA*
[b]*State Key Laboratory of Mechanical Transmissions, College of Automotive Engineering, Chongqing University, Chongqing 400044, People's Republic of China*

This article seeks to derive insight on battery charging control using electrochemistry models. Directly using full order complex multi-partial differential equation (PDE) electrochemical battery models is difficult and sometimes impossible to implement. This article develops an approach for obtaining optimal charge control schemes, while ensuring safety through constraint satisfaction. An optimal charge control problem is mathematically formulated via a coupled reduced order electrochemical-thermal model which conserves key electrochemical and thermal state information. The Legendre-Gauss-Radau (LGR) pseudo-spectral method with adaptive multi-mesh-interval collocation is employed to solve the resulting nonlinear multi-state optimal control problem. Minimum time charge protocols are analyzed in detail subject to solid and electrolyte phase concentration constraints, as well as temperature constraints. The optimization scheme is examined using different input current bounds, and an insight on battery design for fast charging is provided. Experimental results are provided to compare the tradeoffs between an electrochemical-thermal model based optimal charge protocol, an electro-thermal-aging model based balanced charge protocol, and a traditional charge protocol.

Manuscript submitted January 30, 2017; revised manuscript received May 17, 2017. Published 00 0, 2017.

This article develops an approach to solve for optimal charge control schemes using an electrochemical based model with thermal dynamics. The goal is to systematically obtain optimal charge schemes that result in the lowest charge times, while understanding their nature to gain an insight on battery design optimization for fast charging.

Batteries are widely utilized in mobile handsets, electric vehicles (EVs), and power grid energy storage.[1,2] They are an enabling technology for diversifying and securing our future energy supplies. In contrast to simple and rapid refueling of gasoline or diesel, battery recharge requires meticulous control and management, owing to complex electrochemical reactions, immeasurable internal states, and serious safety concerns.[3] Fast charging is a thriving area of research, as it increases the practicality and consumer acceptance of battery-powered devices (e.g., EVs). Nevertheless, it can also impair battery longevity depending on the charging method used, particularly due to heating. It is thus crucial to systematically study the effects of electrochemical and thermal states on charging time, which is the focus of this article.

The traditional charging protocol for Li-ion batteries is constant-current/constant-voltage (CC-CV).[4] In the CC stage, the charging current is constant until a pre-specified voltage threshold is reached, and in the CV stage the voltage threshold is maintained until the current relaxes below a pre-specified threshold value. This technique is simple and easily implemented. The current rate and voltage threshold are, however, almost universally selected in an ad-hoc manner.

In the literature, various methods have been proposed to reduce charge times, such as multi-stage CC (high CC followed by low CC) plus CV (CC-CC-CV),[5,6] boost charging (CV-CC-CV),[7] constant power-constant voltage (CP-CV),[8] fuzzy logic,[9,10] neural networks,[11] gray system theory,[12] and ant colony system algorithm.[13] Alternative protocols were reported to prolong the battery lifetime as well, such as MCC-CV (low CC followed by high CC plus CV)[8] and CC-CV with negative pulse (CC-CV-NP).[14,15] This literature provides enormous insight on rapid charging, but all the protocols are – at some level – heuristic. That is, they employ basic knowledge, empirical observations, and experience of the battery's electrical properties to devise a charging strategy. Their implementation and performance are subject to cumbersome meta-parameter tuning. Furthermore, there are no mathematical guarantees for fast charge optimality, nor constraint satisfaction.

Recently, some researchers have given first insights into model-based optimal charge control.[16–22] A significant challenge for model-based charge control is numerically solving a multi-state nonlinear calculus of variations optimal control problem. These previous studies side-step this difficulty using linear-quadratic formulations,[16] state independent electrical parameters,[17] piecewise constant time discretization,[18] linear input-output models,[19,20] a one-step model predictive control formulation,[21] or a reference governor formulation.[22] To directly face the nonlinear variational calculus problem, orthogonal collocation enabled pseudo-spectral methods were employed in Ref. 23 to optimize charging time and efficiency of lithium-ion batteries. This work was extended in Refs. 24,25 to consider aging and coupled electrical-thermal dynamics via equivalent circuit type models. However, all of the foregoing studies do not explore coupled and fully constrained electrochemical-thermal dynamics for fast charge applications which can lead to overly conservative or unsafe operation.[22] Moreover, previous model based techniques do not give insight on what parameters a battery cell designer can optimize for enabling faster charge times.

This article pursues a different approach to developing optimal fast charging protocols using electrochemical-thermal models. Mathematically, we formulate a minimum time optimal control problem via a coupled single particle model with electrolyte and thermal dynamics (SPMeT). In the coupled model, two PDE single particle subsystems capture both anode and cathode solid concentration dynamics, a three-PDE electrolyte subsystem captures the electrolyte concentration dynamics in three domains (anode, separator, cathode) which all feed into the nonlinear voltage output function.[10] The nonlinear voltage output and bulk solid concentrations are then fed into the two-state thermal subsystem,[14] whose temperature feeds back into the nonlinear voltage output and solid/electrolyte dynamics. Due to the coupled electrochemical-thermal dynamics, the optimization problem is highly nonlinear. Consequently, there are no analytic solutions and numerical solutions have been considered extremely difficult. We challenge this entrenched mindset by leveraging the Legendre-Gauss-Radau (LGR) pseudo-spectral method with adaptive multi-mesh-interval collocation. It is also worth emphasizing that incorporating a two-state temperature model in lieu of the commonly-used single lumped temperature yields more accurate predictions and safer charging protocols as it is known that the core temperature of a cell can be higher than the surface temperature under high current rates.[31] To the best of the authors' knowledge, it is the first minimum time charging optimization framework that uses an experimentally validated electrochemical-thermal model (via measured voltage and temperature) for charging subject to both electrochemical and thermal limits.

This article extends our previous work[26] with: (i) the incorporation of temperature dependent electrochemical model parameters

[z]E-mail: heperez@berkeley.edu

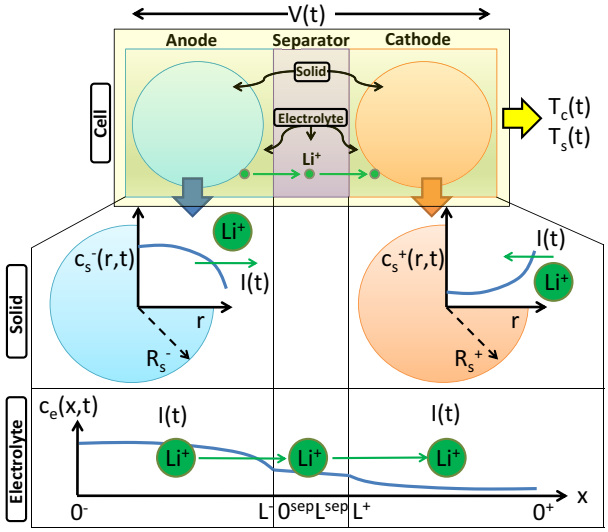

Figure 1. Each electrode is idealized as a single porous spherical particle whose dynamics evolve in the r dimension. The electrolyte concentration dynamics evolve in all regions in the x dimension.

and a two state thermal model, (ii) an experimental validation of the electrochemical-thermal model dynamics for charging, (iii) analysis of optimal charge protocols using the validated electrochemical-thermal model, and (iv) experimental comparison and tradeoff analysis of capacity fade and charging time for an electrochemical-thermal model based optimal charge protocol, an electro-thermal-aging model based balanced charge protocol , and a traditional CC-CV charge protocol.

The remainder of this article is structured as follows. In the second section, the single particle model with electrolyte and thermal dynamics is described. In the third section, the minimum time optimal charge control problem is formulated, and the LGR pseudo-spectral method is briefly introduced. Optimization results are discussed in the fourth section, followed by experimental results in the fifth section. Finally, the sixth section concludes with a summary of the key findings.

Single Particle Model with Electrolyte and Thermal Dynamics

The SPMeT is summarized in this section. The single particle model with electrolyte dynamics (SPMe) used here is most similar to[27–29] and achieves a higher prediction accuracy than the single particle model (SPM) without electrolyte dynamics. Complete details on the derivation and model properties of the SPMe are presented in Ref. 30. The thermal model from Refs. 31,32 is coupled to the SPMe to form the SPMeT (see Fig. 1).

SPMeT model.—The SPMeT model consists of: (i) two linear spherical diffusion PDEs modeling each electrode's solid concentration dynamics, (ii) a quasilinear diffusion equation (across three domains) modeling the electrolyte concentration dynamics, (iii) a nonlinear output function mapping boundary values of solid concentration, electrolyte concentration, and current to terminal voltage, and (iv) two ODEs modeling the core and surface temperature of the cell. The average temperature then feeds back into the nonlinear output function, and the solid and electrolyte dynamics (see Fig. 2).

We now introduce the SPMeT equations. The solid diffusion Equations 1 with boundary conditions 2 are

$$\frac{\partial c_s^{\pm}}{\partial t}(r,t) = \frac{1}{r^2}\frac{\partial}{\partial r}\left[D_s^{\pm}(T_{avg})r^2\frac{\partial c_s^{\pm}}{\partial r}(r,t)\right], \quad [1]$$

$$\frac{\partial c_s^{\pm}}{\partial r}(0,t) = 0, \quad \frac{\partial c_s^{\pm}}{\partial r}(R_s^{\pm},t) = \mp\frac{1}{D_s^{\pm}(T_{avg})Fa^{\pm}L^{\pm}}I(t). \quad [2]$$

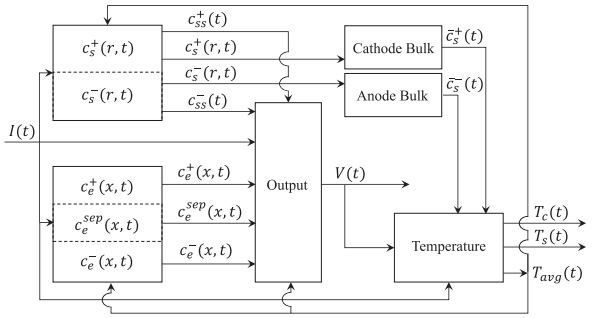

Figure 2. Block diagram of SPMeT. Note that the c_s^+, c_s^-, c_e subsystems are independent of one another. However, all subsystems are coupled through temperature since it feeds back into the nonlinear voltage output and c_s^+, c_s^-, c_e subsystems.

The Neumann boundary conditions at $r = R_s^{\pm}$ signify the flux entering the electrode is proportional to the input current $I(t)$ (positive for charge). The Neumann boundary conditions at $r = 0$ are spherical symmetry conditions and required for well-posedness. Next, the electrolyte diffusion Equations 3–5 with boundary conditions 6–9 are

$$\varepsilon_e^{-}\frac{\partial c_e^{-}}{\partial t}(x,t) = \frac{\partial}{\partial x}\left[D_e^{eff}(c_e^{-},T_{avg})\frac{\partial c_e^{-}}{\partial x}(x,t)\right] - \frac{(1-t_c^0)}{FAL^{-}}I(t), \quad [3]$$

$$\varepsilon_e^{sep}\frac{\partial c_e^{sep}}{\partial t}(x,t) = \frac{\partial}{\partial x}\left[D_e^{eff}(c_e^{sep},T_{avg})\frac{\partial c_e^{sep}}{\partial x}(x,t)\right], \quad [4]$$

$$\varepsilon_e^{+}\frac{\partial c_e^{+}}{\partial t}(x,t) = \frac{\partial}{\partial x}\left[D_e^{eff}(c_e^{+},T_{avg})\frac{\partial c_e^{+}}{\partial x}(x,t)\right] + \frac{(1-t_c^0)}{FAL^{+}}I(t), \quad [5]$$

$$\frac{\partial c_e^{-}}{\partial x}(0^{-},t) = \frac{\partial c_e^{+}}{\partial x}(0^{+},t) = 0, \quad [6]$$

$$D_e^{eff}(L^{-},T_{avg})\frac{\partial c_e^{-}}{\partial x}(L^{-},t) = D_e^{eff}(0^{\text{sep}},T_{avg})\frac{\partial c_e^{sep,}}{\partial x}(0^{\text{sep}},t), \quad [7]$$

$$D_e^{eff}(L^{\text{sep}},T_{avg})\frac{\partial c_e^{sep,}}{\partial x}(L^{\text{sep}},t) = D_e^{eff}(L^{+},T_{avg})\frac{\partial c_e^{+}}{\partial x}(L^{+},t), \quad [8]$$

$$c_e(L^{-},t) = c_e(0^{\text{sep}},t), \quad c_e(L^{\text{sep}},t) = c_e(L^{+},t). \quad [9]$$

The nonlinear output function for terminal voltage is governed by a combination of electric overpotential, electrode thermodynamics, Butler-Volmer kinetics, and electrolyte potential as

$$\begin{aligned} V(t) = {} & \frac{RT_{avg}(t)}{\alpha F}\sinh^{-1}\left(\frac{I(t)}{2a^{+}AL^{+}\bar{i}_0^{+}(t)}\right) \\ & - \frac{RT_{avg}(t)}{\alpha F}\sinh^{-1}\left(\frac{-I(t)}{2a^{-}AL^{-}\bar{i}_0^{-}(t)}\right) \\ & + U^{+}(c_{ss}^{+}(t)) - U^{-}(c_{ss}^{-}(t)) \\ & + \left(\frac{R_f^{+}}{a^{+}AL^{+}} + \frac{R_f^{-}}{a^{-}AL^{-}} + \frac{R_{ce}(T_{avg}(t))}{A}\right)I(t) \\ & + \left(\frac{L^{+}+2L^{\text{sep}}+L^{-}}{2A\bar{\kappa}^{eff}(T_{avg})}\right)I(t) \\ & + k_{\text{conc}}(t)\left[\ln c_e(0^{+},t) - \ln c_e(0^{-},t)\right], \end{aligned} \quad [10]$$

where $c_{ss}^{\pm}(t) = c_s^{\pm}(R_s^{\pm},t)$ is the surface concentration in the solid, $k_{\text{conc}} = \frac{2RT_{avg}(t)}{F}(1-t_c^0)\bar{k}_f(t)$, and $\bar{i}_0^{\pm}(t)$ is the spatially averaged exchange current density

$$i_0^{\pm}(t) = k^{\pm}(T_{avg})\left[c_{ss}^{\pm}(t)\right]^{\alpha_c}\left[c_e^{\pm}(x,t)\left(c_{s,\max}^{\pm} - c_{ss}^{\pm}(t)\right)\right]^{\alpha_a}. \quad [11]$$

The temperature dependent electrochemical parameters follow an Arrhenius law

$$P(T_{avg}) = P_{ref} \exp\left(\frac{E_{ap}}{R}\left(\frac{1}{T_{ref}} - \frac{1}{T_{avg}}\right)\right). \quad [12]$$

The core and surface temperature dynamics of the cylindrical cell are governed by

$$\frac{dT_c(t)}{dt} = \frac{T_s(t) - T_c(t)}{R_c C_c} + \frac{Q(t)}{C_c}, \quad [13]$$

$$\frac{dT_s(t)}{dt} = \frac{T_f(t) - T_s(t)}{R_u C_s} - \frac{T_s(t) - T_c(t)}{R_c C_s} \quad [14]$$

where $Q(t) = I(t)|V(t) - (U^+(\bar{c}_s^+(t)) - U^-(\bar{c}_s^-(t)))|$ is the heat generation including joule heating and energy dissipated by electrode overpotentials and $\bar{c}_s^{\pm}(t)$ is the bulk concentration in the anode/cathode

$$\bar{c}_s^{\pm}(t) = \frac{3}{(R_s^{\pm})^3}\int_0^{R_s^{\pm}} r^2 c_s^{\pm}(r,t)dr. \quad [15]$$

The heat conduction resistance, convection resistance, core heat capacity, and surface heat capacity are represented by R_c, R_u, C_c, and C_s, respectively. The two states are the core T_c and surface T_s temperatures. We assume that the coolant flow rate is constant (which translates to a constant R_u), and the ambient temperature T_f is nearly constant as done in Refs. 31,32. The average cell temperature is

$$T_{avg}(t) = \frac{T_c(t) + T_s(t)}{2}, \quad [16]$$

which is approximately equal to the radial average temperature[33] for the cell considered in this study. The thermal parameters have been identified in previous work.[31,32] We determine R_u using our experimental setup as described in Section.

We define the cell SOC via the bulk SOC (bulk concentration normalized against maximum concentration) and stoichiometric difference in the anode as

$$SOC(t) = \frac{\bar{c}_s^-(t)}{c_{s,max}^-|x_{100\%} - x_{0\%}|}. \quad [17]$$

This cell SOC represents the ratio of available charge to maximum usable charge.

This summarizes the SPMeT which maintains accuracy at higher C-rates than that of an SPM with thermal dynamics alone.[30] The model parameters used in this study originate from Refs. 27,31,34–37 and correspond to a lithium iron phosphate cathode / graphite anode chemistry A123 26650 2.3Ah cell. We determine some parameters based on our experimental setup and validate the effectiveness of the electrochemical-thermal model for various charging cases in Section.

Comparison to existing SPMe models.—The models in Refs. 27–29 are most similar to the SPMe presented here with a few critical differences. In Ref. 27, bulk solid concentration is used in the voltage output function instead of the surface concentration we use here (see (26) in Ref. 27). In the case of Ref. 28 volume averaging is performed in the electrolyte phase which partially obscures electrolyte polarization. In Ref. 29, the authors use an approximation of the solid state diffusion equation instead of retaining the PDE version we use in 1–2 (see Section 2 of Ref. 29). Moreover, we include a temperature submodel, as does.[27]

Optimal Charge Control Formulation

Next we formulate a minimum-time/safe optimal charge control problem. The objective function J is given by

$$\min_{I(t),x(t),t_f} \int_{t_0}^{t_f} 1 \cdot dt, \quad [18]$$

where $(t_f - t_0)$ is the charge time to reach a desired target SOC (SOC_f). The optimization variables are the input current $I(t)$ and final time t_f, with state variables

$$x(t) = [c_s^+(r,t), c_s^-(r,t), c_e^+(x,t), c_e^{sep}(x,t), c_e^-(x,t), T_c(t), T_s(t)]^T. \quad [19]$$

The constraints include the model dynamics and boundary conditions 1–9, input, state, event, and time constraints below:

$$I_{min} \le I(t) \le I_{max}, \quad [20]$$

$$\theta_{min}^{\pm} \le \frac{c_s^{\pm}(r,t)}{c_{s,max}} \le \theta_{max}^{\pm}, \quad [21]$$

$$c_{e,min} \le c_e^l(x,t) \le c_{e,max}, \quad l \in \{-, \text{sep}, +\} \quad [22]$$

$$T_{min} \le T_m(t) \le T_{max}, \quad m \in \{c, s\} \quad [23]$$

$$t_0 \le t_f \le t_{max}, \quad [24]$$

$$c_s^{\pm}(r,t_0) = c_{s,0}^{\pm}, \quad c_e^l(x,t_0) = c_{e,0}^l, \quad l \in \{-, \text{sep}, +\} \quad [25]$$

$$SOC(t_f) = SOC_f, \qquad SOC(t_0) = SOC_0, \quad [26]$$

$$T_m(t_0) = T_0, \quad m \in \{c, s\}. \quad [27]$$

Constraints 21–22 protect the solid active material and electrolyte from lithium depletion/oversaturation. Constraint 23 protects against excessively cold or hot temperatures that accelerate cell aging.

The PDE system 1–9 is discretized in space using a second-order accurate finite central difference method that conserves lithium,[38] resulting in a nonlinear differential algebraic equation system. Due to this complex mathematical structure, it is difficult to use conventional optimization techniques, e.g., dynamic programming, Pontryagin's minimum principle, and indirect methods, due to intractable computational burden or accuracy. Instead, we pursue pseudo-spectral methods to transcribe this infinite-dimensional optimal control problem into a finite-dimensional optimization problem with algebraic constraints at the discretized nodes. Then, the optimization variables at such nodes are solved by off-the-shelf nonlinear programming (NLP) solvers, like SNOPT or IPOPT.[39] Note that convexity is not guaranteed, and therefore these solvers yield locally optimal solutions. Pseudo-spectral methods are an effective tool for complex nonlinear optimal control problems and have been extensively applied to real-world optimization problems in engineering, including aerospace and autonomous flight systems,[40] road vehicle systems,[41] energy storage,[23,24] etc. There are a myriad of approaches for discretizing integral and differential equations, leading to a spectrum of pseudo-spectral variants. In this study, we use the Legendre-Gauss-Radau (LGR) pseudo-spectral method with adaptive multi-mesh-interval collocation, featured by the general purpose optimal control software (GPOPS-II).[39] This software incorporates an orthogonal collocation method to generate the LGR points. Rather than a traditional fixed global mesh, an adaptive mesh refinement algorithm is employed to iteratively adjust the number of mesh intervals, the width of each interval, and the polynomial degree (the number of LGR points). Theoretical and algorithmic properties of this method are elaborated in Refs. 42,43.

Results and Discussion

This section presents optimization results for minimum-time charge in the absence of modeling, measurement, or control uncertainty. It also examines solution sensitivity to perturbations in model parameters.

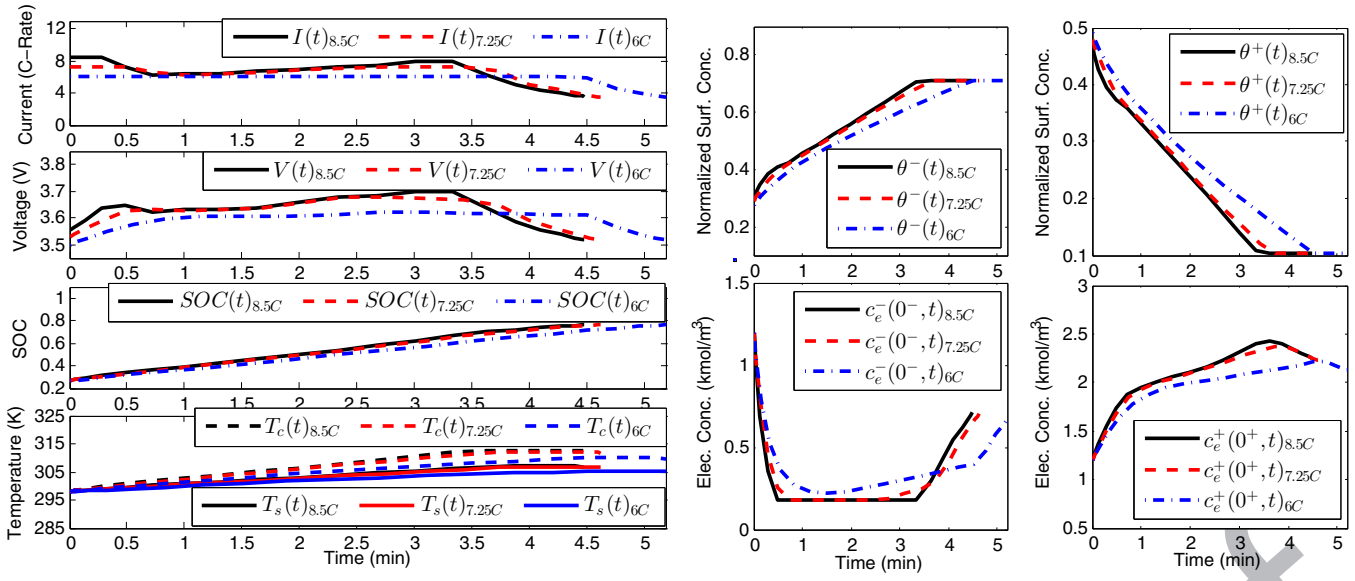

Figure 3. Optimization results for minimum time charge with $I_{max} = \{8.5C, 7.25C, 6C\}$. Left: Current $I(t)$, Voltage $V(t)$, State of Charge $SOC(t)$, Temperatures $T_c(t)$, $T_s(t)$. Right: Surface Concentrations $\theta^-(t)$, $\theta^+(t)$, Electrolyte Concentrations $c_e^-(0^-,t)$, $c_e^+(0^+,t)$.

Minimum time charge.—The optimal charge trajectories are shown in Fig. 3 for $I_{max} = \{8.5C, 7.25C, 6C\}$. It takes 4.4822 min to achieve a target SOC of 75% ($SOC_f = 0.75$) from an initial SOC of 25% ($SOC_0 = 0.25$)[c] when $I_{max} = 8.5C$. The charge process follows a constant-current/constant-electrolyte-concentration/constant-surface-concentration (CC-CCe-CCss) protocol. To minimize charging time, the maximum C-rate is applied initially, causing the minimum electrolyte concentration constraint to become active at the anode current collector. The surface concentration at the anode increases until it reaches its maximum value, which becomes the dominant inequality constraint. A similar behavior is observed when $I_{max} = 7.25C$, with a longer initial current at the maximum C-rate. It takes 4.6174 min to achieve the target SOC in this case, which is slightly more than the previous case. Note that once the the minimum electrolyte concentration constraint becomes active at the anode current collector, the protocol follows almost the same trajectory as the previous case. A slightly different behavior is observed when $I_{max} = 6C$, which just has 2 steps. It takes 5.2016 min to achieve the target SOC in this case, which is longer in time than the previous cases. This protocol follows a constant-current/constant-surface-concentration (CC-CCss) protocol. The maximum C-rate is applied initially, until the maximum surface concentration at the anode constraint becomes active. Heuristically, the first two protocols where $I_{max} = \{8.5C, 7.25C\}$ are similar in nature to the CC-CC-CV charge protocol[5,6] which involves an initial high constant current period, followed by a lower constant current period, and then by a constant voltage period. The last protocol where $I_{max} = 6C$ is similar in nature to the well known CC-CV protocol.[4]

A comparison of the optimized charge protocol vs. a CC-CC-CV protocol ($CC_1 = 7.25C$, $CC_2 = 5.75C$) is presented in Fig. 4 for $I_{max} = 7.25C$. We make two observations. (i) It takes the CC-CC-CV protocol 5.2233 min to achieve the target SOC, a 0.6059 min (13.12%) increase w.r.t. the optimized charge protocol at $I_{max} = 7.25C$. (ii) The optimized protocol allows safe excursions beyond the 3.6 V upper limit in CC-CC-CV by ensuring the electrochemical state constraints are satisfied. Not only is the optimized protocol (with $I_{max} = 7.25C$) faster than the CC-CC-CV protocol here, it allows for safe charging since the CC-CC-CV protocol violates the surface concentration constraints at the anode and cathode chosen in this study.

Similarly, a comparison of the optimized charge protocol vs. the well known CC-CV ($CC = 6C$) protocol is presented in Fig. 5 for $I_{max} = 6C$. We make similar observations. (i) It takes the CC-CV protocol 5.2733 min to achieve the target SOC, a 0.0717 min (1.37%) increase w.r.t. the optimized charge protocol at $I_{max} = 6C$. (ii) The optimized protocol allows safe excursions beyond the 3.6 V upper limit in CC-CV by ensuring the electrochemical state constraints are satisfied. Although the optimized protocol (with $I_{max} = 6C$) is not significantly faster than the CC-CV protocol here, it allows for safe charging since the CC-CV protocol violates the surface concentration constraints at the anode and cathode chosen in this study.

Sensitivity based battery design for fast charging.—Next we examine the solution sensitivity to small perturbations in nominal model parameters for fast charging (while maintaining similar optimal charge protocols). In previous results, we noted that the first electrochemical constraint to become active was the electrolyte concentration at the anode current collector when $I_{max} = \{8.5C, 7.25C\}$. This observation motivates exploring how alterations to the electrolyte dynamics impact minimum charge time. We also explore how changes in other model parameters affect the minimum charge time.

Electrolyte Diffusivity $D_e(c_e, T_{avg})$.—A comparison between the optimized charge protocol for a $\pm 2.5\%$ deviation in $D_e(c_e, T_{avg})$ and the solution with nominal parameters is shown in Fig. 6 for $I_{max} = 8.5C$. The optimized charge protocol with a $+2.5\%$ deviation requires 4.4002 min to achieve the target SOC. The cell with greater electrolyte diffusivity requires 0.082 min (1.83%) less charge time. Consequently, increasing $D_e(c_e, T_{avg})$ is favorable to obtaining a faster charge time. The optimized charge protocol with a -2.5% deviation requires 4.5660 min to achieve the target SOC. The cell with lower electrolyte diffusivity requires 0.0838 min (1.87%) more charge time. Consequently, decreasing $D_e(c_e, T_{avg})$ is not favorable to obtaining a faster charge time. Note that the trajectories are similar to that of the unperturbed solution. The difference is seen in the electrolyte concentration dynamics which become faster or slower depending on the increase or decrease in $D_e(c_e, T_{avg})$, respectively.

[c]The initial SOC is chosen at 25% since this is near the point where electric vehicles and consumer electronics (e.g. mobile phones, tablets, and laptops) begin to indicate that the battery is low. The final SOC is chosen at 75% to represent where the battery would have enough energy stored to complete desired tasks before the next charge with a charge time close to 5 minutes (comparable to the time it takes to refuel a vehicle with gasoline or time it takes to get a beverage while charging a mobile device).

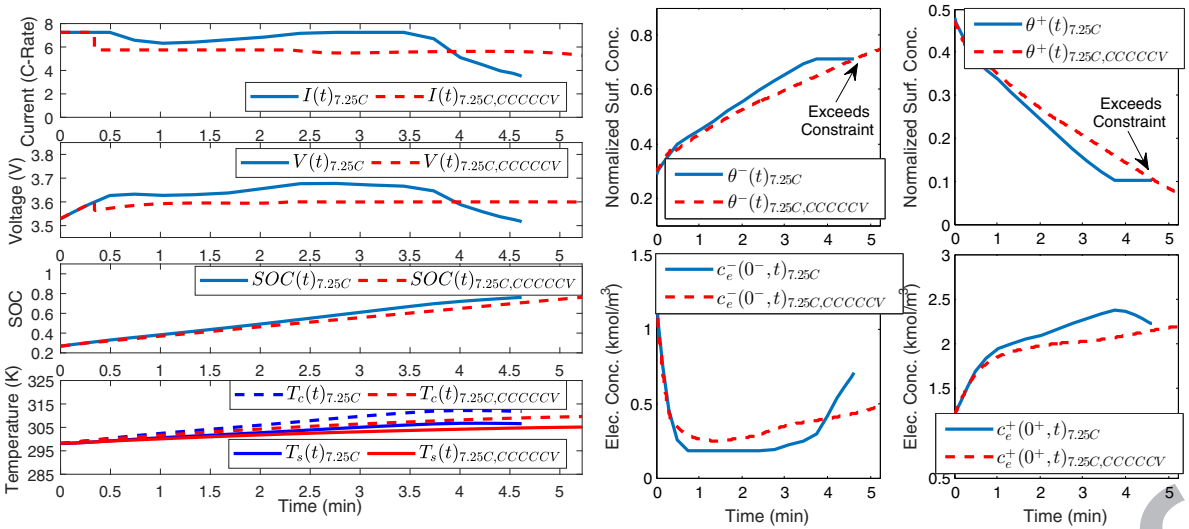

Figure 4. Optimized charge vs. CC-CC-CV charge trajectories with $I_{max} = 7.25C$. Left: Current $I(t)$, Voltage $V(t)$, State of Charge $SOC(t)$, Temperatures $T_c(t)$, $T_s(t)$. Right: Surface Concentrations $\theta^-(t)$, $\theta^+(t)$, Electrolyte Concentrations $c_e^-(0^-,t)$, $c_e^+(0^+,t)$.

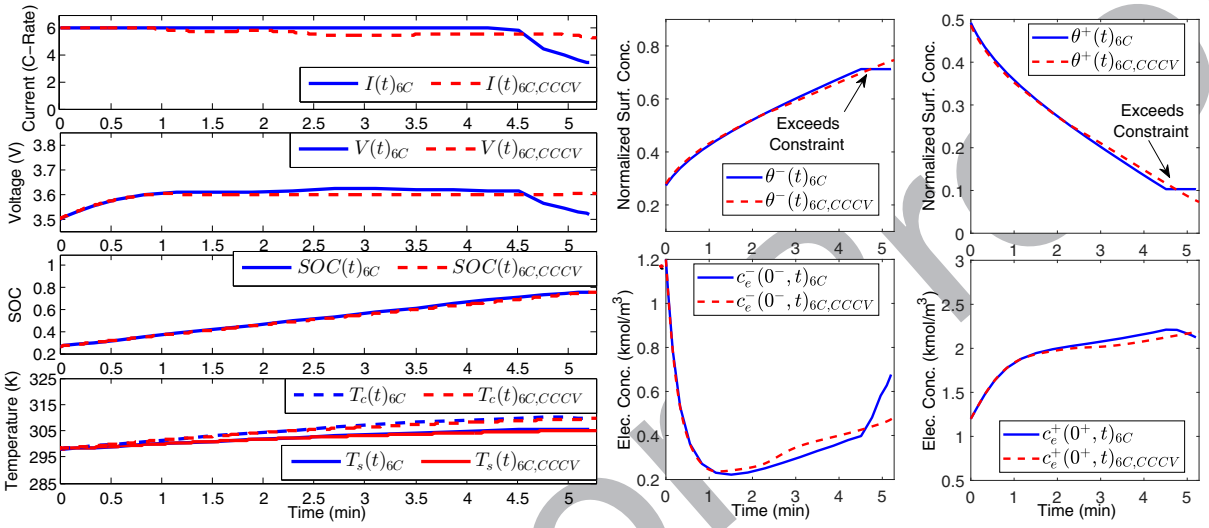

Figure 5. Optimized charge vs. CC-CV charge trajectories with $I_{max} = 6C$. Left: Current $I(t)$, Voltage $V(t)$, State of Charge $SOC(t)$, Temperatures $T_c(t)$, $T_s(t)$. Right: Surface Concentrations $\theta^-(t)$, $\theta^+(t)$, Electrolyte Concentrations $c_e^-(0^-,t)$, $c_e^+(0^+,t)$.

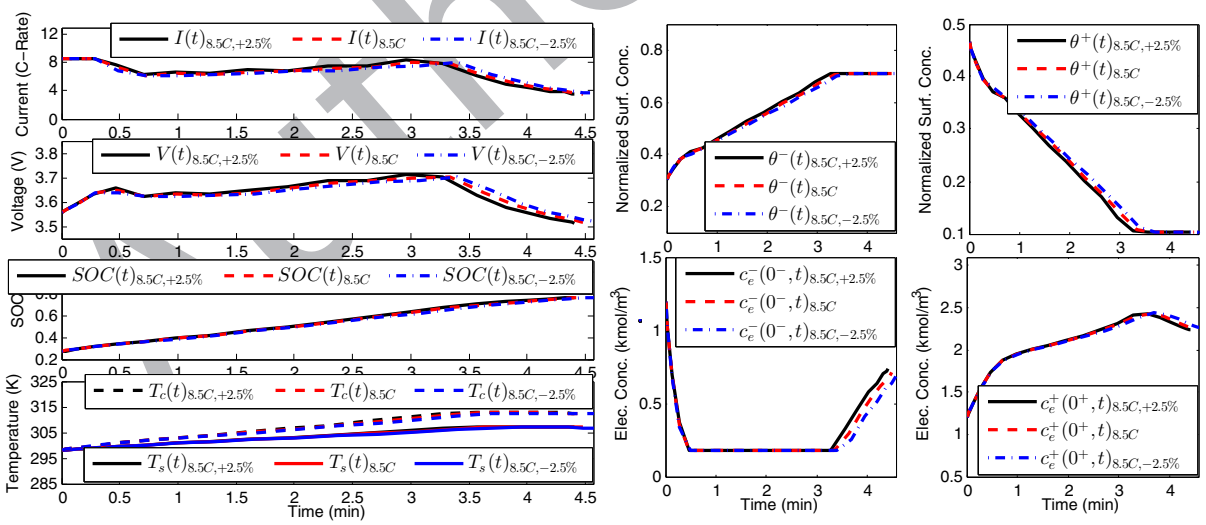

Figure 6. Influence of a $\pm 2.5\%$ deviation in $D_e(c_e, T_{avg})$ on optimization results for minimum time charge with $I_{max} = 8.5C$. Left: Current $I(t)$, Voltage $V(t)$, State of Charge $SOC(t)$, Temperatures $T_c(t)$, $T_s(t)$. Right: Surface Concentrations $\theta^-(t)$, $\theta^+(t)$, Electrolyte Concentrations $c_e^-(0^-,t)$, $c_e^+(0^+,t)$.

Table I. Minimum charge times for perturbed solutions.

Parameter	Chg. Time (+2.5%)	Chg. Time (−2.5%)
t_c^0	4.4317 min	4.5313 min
$D_s^+(T_{avg})$	4.4796 min	4.5268 min
R_s^+	4.5837 min	4.4803 min
R_u	4.4748 min	4.4899 min

Other parameters t_c^0, $D_s^+(T_{avg})$, R_s^+, R_u.—Similarly, we examine the impact of the transference number t_c^0, solid diffusivity of the cathode $D_s^+(T_{avg})$, solid particle radius of the cathode R_s^+, and cooling convection coefficient R_u on the minimum charge time. The results are summarized in Table I. Note that an increase in the transference number t_c^0, solid diffusivity of the cathode $D_s^+(T_{avg})$, and cooling convection coefficient R_u is favorable to obtaining a faster charge time. However, an increase in the solid particle radius of the cathode R_s^+ is not favorable to obtaining a faster charge time.

An increase in the transference number t_c^0 effectively scales down the input current to the electrolyte diffusion dynamics which translates to a higher current allowed for fast charging before the constraint is reached. Increasing the solid diffusivity of the cathode $D_s^+(T_{avg})$ speeds up the solid diffusion dynamics, and scales down the input current at the boundary which allows for a higher current when fast charging before the constraint is reached. Furthermore, increasing the cooling convection coefficient R_u means there is less cooling of the battery which translates to higher overall temperatures that is favorable for fast charging (since the dynamics of the solid and electrolyte speed up, and overall resistance of the cell goes down).

Experimental Results and Discussion

Various experiments were conducted to validate the electrochemical-thermal model constructed in this article using parameters from Refs. 27,31,34–37 for a 2.3Ah A123 Systems 26650 $LiFePO_4$ battery in our test facility. The cell was placed on an Arbin High Current Cylindrical Cell Holder inside of an ESPEC BTL-433 environmental chamber to regulate the ambient temperature at 25^oC (298.15 K). A K-type thermocouple was placed on the surface of the battery to measure T_s. First, the cell was cycled using a C/20 CC-CV test to identify open circuit voltage (OCV) (and open circuit potential (OCP) of the cathode and anode) using a PEC SBT2050 cycler that controls the input current to the battery. Then a 5C CC-CV charge test was performed to identify some electrochemical-thermal parameters for our experimental setup. The resulting SPMeT optimal charge protocols with $I_{max} = \{8.5C, 7.25C, 6C\}$ from the optimization results (using the newly determined open circuit potentials and electrochemical-thermal parameters) are then applied to the battery for validation of the output voltage and surface temperature of the electrochemical-thermal model. We experimentally compare the SPMeT optimal charge protocol with $I_{max} = 6C$ against a 5C CC-CV charge protocol (C-rate chosen based on higher charge time) on two cells. The two cells undergo several hundred cycles to determine the changes in capacity fade and charge time.

Electrochemical-thermal model validation.—The open circuit voltage is determined by taking the average of the charge and discharge voltage curves from a C/20 CC-CV cycling test (with voltage limits of 3.6 V and 2.0 V), and is used to determine the open circuit potentials ($U^{\pm}$) based on OCPs from literature[37] of the cathode and anode (shown in Fig. 7) that minimize the root mean square error between the modeled and experimental OCV. Then a 5C CC-CV charge protocol was applied to the battery to determine electrochemical-thermal model parameters ($R_s^{\pm}$, $\epsilon_e^{\pm}$, $D_e(c_e, T_{avg})$, R_{ce}) that minimize the root mean square error between the modeled and experimental voltage and surface temperature. The initial and final conditions of the applied 5C CC-CV charge protocol were 25% SOC and 25^oC (298.15 K), and 75% SOC and 31.45^oC (304.6 K), respectively.

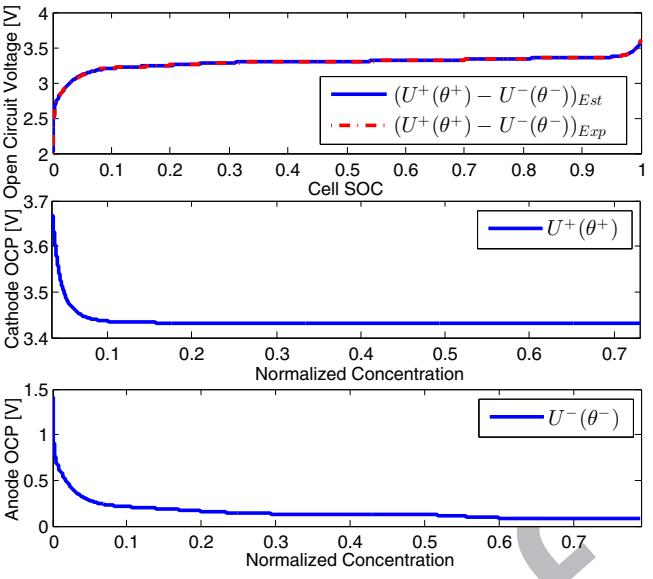

Figure 7. Experimental Determination of Open Circuit Potentials from Open Circuit Voltage: Estimated Open Circuit Voltage $(U^+(\theta^+) - (U^-(\theta^-))_{Est}$, Experimental Open Circuit Voltage $(U^+(\theta^+) - U^-(\theta^-))_{Exp}$, Cathode Open Circuit Potential $U^+(\theta^+)$, and Anode Open Circuit Potential $U^-(\theta^-)$.

The current profiles for the SPMeT optimal charge optimization results with $I_{max} = \{8.5C, 7.25C, 6C\}$ are then applied (open loop) to validate the voltage and surface temperature of the electrochemical-thermal model, as shown in Figs. 8–10 which achieves a Voltage RMSE of {25.9 mV, 23.9 mV, 16.3 mV} and a Surface Temperature RMSE of {0.1598 K, 0.1703 K, 0.3733 K}, respectively.

Charge protocol aging.—Two cells were used to determine the tradeoffs between capacity fade and charge time for a fixed 1.15Ah charge throughput (using the SPMeT optimal charge protocol with $I_{max} = 6C$ and 5C CC-CV charge protocols). Both cells are discharged with a 1C CC-CV protocol to the open circuit voltage corresponding to 25% SOC. The charge and discharge protocol of each

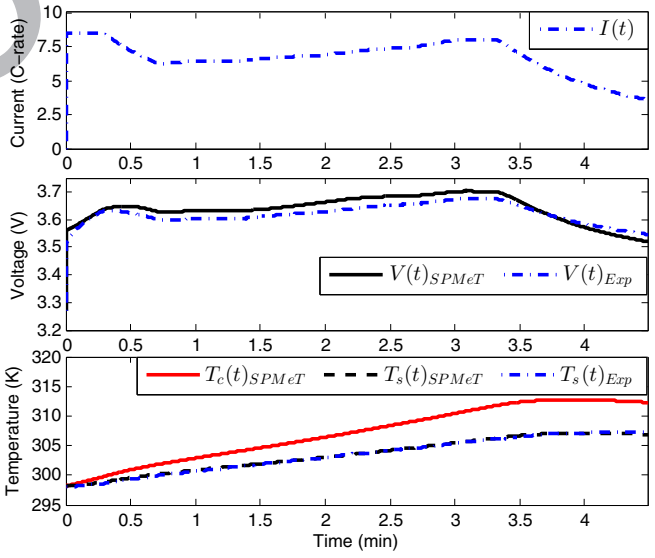

Figure 8. Experimental Validation of Electrochemical-Thermal Model via SPMeT Optimal Charge Protocol when $I_{max} = 8.5C$: Current $I(t)$, Model Voltage $V(t)_{SPMeT}$, Experimental Voltage $V(t)_{Exp}$, Model Temperatures $T_c(t)_{SPMeT}$, $T_s(t)_{SPMeT}$, and Experimental Temperature $T_s(t)_{Exp}$.

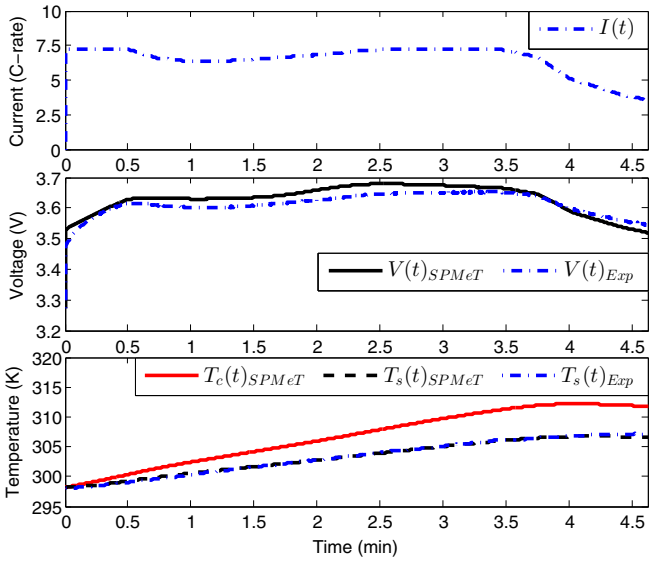

Figure 9. Experimental Validation of Electrochemical-Thermal Model via SPMeT Optimal Charge Protocol when $I_{max} = 7.25C$: Current $I(t)$, Model Voltage $V(t)_{SPMeT}$, Experimental Voltage $V(t)_{Exp}$, Model Temperatures $T_c(t)_{SPMeT}$, $T_s(t)_{SPMeT}$, and Experimental Temperature $T_s(t)_{Exp}$.

cell is then repeated for hundreds of cycles. The current from the SPMeT optimal charge protocol with $I_{max} = 6C$ is applied to the first battery cell (open loop). The 5C CC-CV charge protocol is applied to the second battery cell (closed loop), using the built-in controller of the battery cycler to maintain the 3.6 V limit under the 5C CC-CV charge operation. That is, the same current is applied each time for the SPMeT optimal charge protocol with $I_{max} = 6C$ (regardless of what voltage is measured) while the current for the CC-CV protocol is adjusted in real-time once the voltage constraint becomes active. It is important to highlight that only the CC-CV protocol provides compensation as the cell degrades.

The discharge capacity is determined using a 1C CC-CV cycling test at cycles {0, 10, 60, 110, 160, 210} and is shown (normalized against initial capacity) in the first subplot of Fig. 11. The normalized

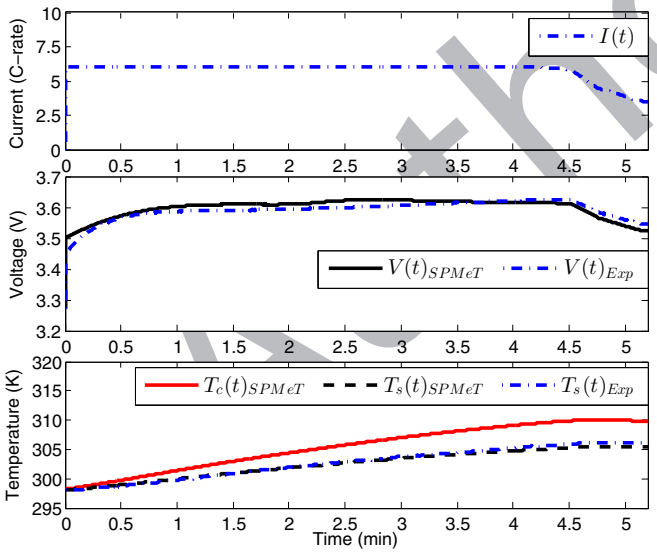

Figure 10. Experimental Validation of Electrochemical-Thermal Model via SPMeT Optimal Charge Protocol when $I_{max} = 6C$: Current $I(t)$, Model Voltage $V(t)_{SPMeT}$, Experimental Voltage $V(t)_{Exp}$, Model Temperatures $T_c(t)_{SPMeT}$, $T_s(t)_{SPMeT}$, and Experimental Temperature $T_s(t)_{Exp}$.

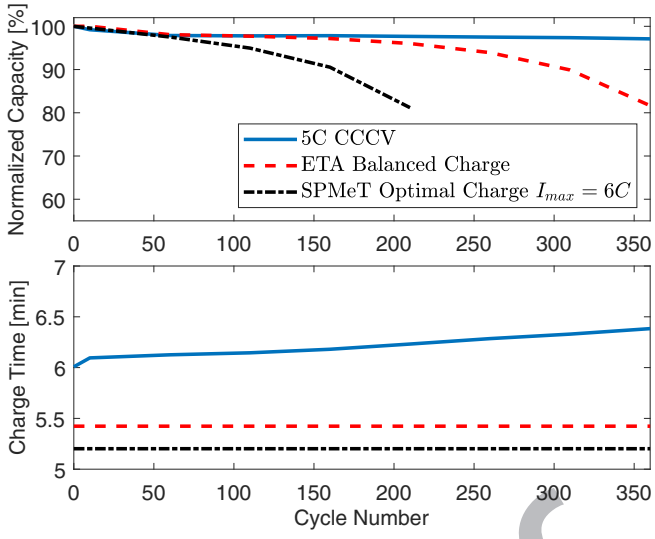

Figure 11. SPMeT Optimal Charge with $I_{max} = 6C$ (Open Loop), ETA Balanced Charge (Open Loop), and 5C CC-CV Charge Protocol (Closed Loop) Aging: Capacity Fade, and Charge Time.

capacity of the SPMeT optimal charge protocol with $I_{max} = 6C$ is 81.18% while that of the 5C CC-CV charge protocol is 97.67% at cycle 210. The higher capacity fade experienced by the SPMeT optimal charge protocol with $I_{max} = 6C$ over the entire 210 cycles is expected since it is applied in a pure open loop fashion (does not compensate for the cell violating electrochemical-thermal constraints as it is cycled) and has a faster charge time than that of the 5C CC-CV protocol. The charge time of the SPMeT optimal charge protocol with $I_{max} = 6C$ stays the same each time while that of the 5C CC-CV protocol increases (due to the closed loop compensation which limits the cell voltage from going above its upper limit as it is cycled) as shown in the bottom subplot of Fig. 11. The charge time of the SPMeT optimal charge protocol with $I_{max} = 6C$ is 5.202 minutes while that of the 5C CC-CV charge protocol is initially 6.008 minutes. The charge time of the 5C CC-CV charge protocol increases to 6.232 minutes at cycle 210. There is a clear tradeoff between degradation and charge time between the SPMeT optimal charge protocol (open loop) with $I_{max} = 6C$ and 5C CC-CV charge protocol (closed loop) that are applied over time. It is important to highlight that the SPMeT optimal charge protocol with $I_{max} = 6C$ provides a faster charge time with a comparable capacity fade to that of the 5C CC-CV charge protocol up to cycle 60.

The capacity fade and charge time results of an electro-thermal-aging (ETA) model based balanced (optimal tradeoff between charge time and aging subject to electrical-thermal-aging constraints) charge protocol (open loop) from Ref. 25 are also presented in Fig. 11 for the cell under study. The discharge capacity is found in a similar fashion at cycles {0, 10, 60, 110, 160, 210, 260, 310, 360} until 81.67% of the normalized capacity for the cell under the ETA model based balanced charge protocol. We note that the capacity fade for the ETA model based balanced charge protocol (open loop) is less compared to the SPMeT optimal charge protocol (open loop) with $I_{max} = 6C$ but higher than the 5C CC-CV charge protocol (closed loop). The charge time of the ETA model based balanced charge protocol (open loop) is slightly higher than the SPMeT optimal charge protocol (open loop) but lower than the 5C CC-CV charge protocol (closed loop). In this case, the ETA model based balanced charge protocol provides a faster charge time with a comparable capacity fade to that of the 5C CC-CV charge protocol up to cycle 110. A cause for the higher capacity fade experienced by the SPMeT optimal charge protocol (open loop) versus the ETA model based balanced charge protocol (open loop) is that we do not directly optimize for both charge time and aging in this study as done in Ref. 25.

These results provide motivation and justification for adaptive closed loop charge control to alleviate aging and provide the optimal charge time performance over time. This closed loop controller would continuously estimate parameters that age with time to yield accurate electrochemical-thermal model estimates for: i) constraint satisfaction to ensure battery safety and longevity, and ii) obtaining new optimal charge protocols as the cell is cycled using the optimal charging control framework shown in this article. With such controller in place, specific degradation mechanisms that occur with cycling can be analyzed and compared (for multiple cells and charge protocols) to evaluate the effectiveness of such adaptive closed loop optimal charging control strategy.

Conclusions

An optimal control framework for a PDE system has been developed to explore model-based fast-safe charging protocols. In this framework, a coupled single particle model with electrolyte and thermal dynamics is incorporated to account for solid and electrolyte phase concentration constraints, as well as thermal constraints. The Legendre-Gauss-Radau (LGR) pseudo-spectral method with adaptive multi-mesh-interval collocation is leveraged to solve the infinite dimensional nonlinear optimal control problem.

Charge time is examined subject to both electrochemical and thermal constraints. The resulting minimum time charge regimes with varying input current limits are analyzed in detail, with the following key findings: (i) The protocol is constant-current/constant-electrolyte-concentration/constant-surface-concentration (CC-CCe-CCss), requiring 4.4822 minutes and 4.6174 minutes to charge the battery from 25% to 75% SOC when $I_{max} = \{8.5C, 7.25C\}$, respectively. This optimized protocol is similar to the heuristic high constant current-low constant current-constant voltage (CC-CC-CV) protocol. (ii) The protocol is constant-current/constant-surface-concentration (CC-CCss) when $I_{max} = 6C$, requiring 5.2016 minutes to charge the battery and is similar to the well known constant-current/constant-voltage (CC-CV) protocol. (iii) The protocol solutions yield physical insight on which battery design parameters to optimize for fast charging applications. Increasing electrolyte diffusivity coefficient $D_e(c_e)$ results in faster charge time when $I_{max} = 8.5C$. Finally, experimental validation results of the SPMeT optimal charge protocol with $I_{max} = 6C$ (open loop) versus an ETA model based balanced charge protocol (open loop) and a 5C CC-CV charge protocol (closed loop) are presented with respect to capacity fade and charge time.

In this paper we assume full state measurements and known parameters to ascertain the maximum possible fast charging benefits of SPMeT-based control. Future work combines the SPMeT presented here with state and parameter estimates generated by adaptive PDE observers.[1] This output feedback system (i) guards against harmful operating regimes, (ii) increases charging speed, and (iii) monitors state-of-charge and state-of-health, all from measurements of voltage, current, and temperature. Future work also includes incorporation of progressive aging dynamics, similar to.[24,25] Finally, we plan to experimentally quantify the aforementioned benefits of the closed loop system in a battery-in-the-loop test facility.

List of Symbols

$L^{\pm}$	Thickness of Cathode/Anode [m]
L^{sep}	Thickness of Separator [m]
A	Electrode Area [m^2]
$R_s^{\pm}$	Radius of Solid Particles in Cathode/Anode [m]
$\epsilon_e^{\pm}$	Volume Fraction of Electrolyte in Cathode/Anode
ϵ_e^{sep}	Volume Fraction of Electrolyte in Separator
$\epsilon_s^{\pm}$	Volume Fraction of Solid in Cathode/Anode
$a^{\pm}$	Specific Interfacial Surface Area of Cathode/Anode [m^2/m^3]
$D_s^{\pm}$	Diffusion Coefficient for Solid in Cathode/Anode [m^2/s]
D_e^{eff}	Effective Diffusion Coefficient for Electrolyte [m^2/s]
t_c^0	Transference Number
F	Faraday's Constant [C/mol]
R	Gas Constant [J/mol-K]
$\alpha_{c,a}$	Charge Transfer Coefficient for Cathode/Anode
$R_f^{\pm}$	Film Resistance in Cathode/Anode [Ωm^2]
R_{ce}	Current Collector/External Resistance [Ωm^2]
$k^{\pm}$	Reaction Rate in Cathode/Anode [$(A/m^2)(mol^3/mol)^{(1+\alpha)}$]
$c_{s,max}^{\pm}$	Max Concentration in Cathode/Anode [mol/m^3]
E_a	Activation Energy [J/mol]
P_{ref}	Reference Parameter Value [-]
Q	Heat Generation [W]
C_c	Lumped Heat Capacity of Core [J/K]
C_s	Lumped Heat Capacity of Surface [J/K]
R_c	Conduction Resistance [K/W]
R_u	Convection Resistance [K/W]
T_f	Ambient Temperature [K]
T_c	Core Temperature [K]
T_s	Surface Temperature [K]
T_{avg}	Average Temperature [K]
T_{ref}	Reference Temperature [K]
I_{min}	Minimum Current [A]
I_{max}	Maximum Current [A]
$\theta_{min}^{\pm}$	Minimum Normalized Concentration in Cathode/Anode
$\theta_{max}^{\pm}$	Maximum Normalized Concentration in Cathode/Anode
$c_{e_{min}}$	Minimum Electrolyte Concentration [mol/m^3]
$c_{e_{max}}$	Maximum Electrolyte Concentration [mol/m^3]
T_{min}	Minimum Cell Temperature [K]
T_{max}	Maximum Cell Temperature [K]
t_f	Charge Time [sec]
$c_s^{\pm}$	Lithium Concentration in the Solid [mol/m^3]
c_e	Lithium Concentration in the Electrolyte [mol/m^3]
$c_{ss}^{\pm}$	Concentration at Particle Surf. in Cathode/Anode [mol/m^3]
$i_0^{\pm}$	Exchange Current Density [A/m^2]
$U^{\pm}$	Open Circuit Potential in the Cathode/Anode [V]
V	Voltage [V]
I	Applied Current [A]
$\bar{c}_s^{\pm}$	Particle Vol. Avg. Concentration in Cathode/Anode [mol/m^3]
$\theta^{\pm}$	Normalized Concentration in Cathode/Anode
SOC	State of Charge

References

1. S. J. Moura, N. Chaturvedi, and M. Krstic, "Adaptive PDE Observer for Battery SOC/SOH Estimation via an Electrochemical Model," *ASME Journal of Dynamic Systems, Measurement, and Control*, **136**, 011015 (2014).
2. X. Hu, N. Murgovski, L. Johannesson, and B. Egardt, "Comparison of Three Electrochemical Energy Buffers Applied to a Hybrid Bus Powertrain With Simultaneous Optimal Sizing and Energy Management," *IEEE Transactions on Intelligent Transportation Systems*, **15**, 1193 (2014).
3. M. Yilmaz and P. Krein, "Review of Battery Charger Topologies, Charging Power Levels, and Infrastructure for Plug-In Electric and Hybrid Vehicles," *IEEE Transactions on Power Electronics*, **28**, 2151 (2013).
4. S. Zhang, K. Xu, and T. Jow, "Study of the charging process of a LiCoO2-based Li-ion battery," *Journal of Power Sources*, **160**(2) 1349 (2006).
5. D. Ansean, M. Gonzalez, J. Viera, V. Garcia, C. Blanco, and M. Valledor, "Fast charging technique for high power lithium iron phosphate batteries: A cycle life analysis," *Journal of Power Sources*, **239**(0), 9 (2013).
6. D. Ansean, M. Dubarry, A. Devie, B. Y. Liaw, V. M. Garcia, J. C. Viera, and M. Gonzalez, "Fast charging technique for high power LiFePO4 batteries: A mechanistic analysis of aging," *Journal of Power Sources*, **321**(0), 201 (2016).
7. P. Notten, J. O. het Veld, and J. van Beek, "Boostcharging Li-ion batteries: A challenging new charging concept," *Journal of Power Sources*, **145**(1), 89 (2005).
8. S. S. Zhang, "The effect of the charging protocol on the cycle life of a Li-ion battery," *Journal of Power Sources*, **161**(2), 1385 (2006).
9. H. Surmann, "Genetic optimization of a fuzzy system for charging batteries," *IEEE Transactions on Industrial Electronics*, **43**, 541 (1996).

10. Y.-H. Liu and Y.-F. Luo, "Search for an optimal rapid-charging pattern for li-ion batteries using the taguchi approach," *IEEE Transactions on Industrial Electronics*, **57**, 3963 (2010).
11. Z. Ullah, B. Burford, and S. Dillip, "Fast intelligent battery charging: neural-fuzzy approach," *IEEE Aerospace and Electronic Systems Magazine*, **11**, 26 (1996).
12. L.-R. Chen, R. Hsu, and C.-S. Liu, "A design of a gray-predicted li-ion battery charge system," *IEEE Transactions on Industrial Electronics*, **55**, 3692 (2008).
13. Y.-H. Liu, J.-H. Teng, and Y.-C. Lin, "Search for an optimal rapid charging pattern for lithium-ion batteries using ant colony system algorithm," *IEEE Transactions on Industrial Electronics*, **52**, 1328 (2005).
14. M. A. Monem, K. Trad, N. Omar, O. Hegazy, B. Mantels, G. Mulder, P. V. den Bossche, and J. V. Mierlo, "Lithium-ion batteries: Evaluation study of different charging methodologies based on aging process," *Applied Energy*, **152**(0), 143 (2015).
15. M. A. Monem, K. Trad, N. Omar, O. Hegazy, P. V. den Bossche, and J. V. Mierlo, "Influence analysis of static and dynamic fast-charging current profiles on aging performance of commercial lithium-ion batteries," *Energy*, **120**(0), 179 (2017).
16. Y. Parvini and A. Vahidi, "Maximizing Charging Efficiency of Lithium-Ion and Lead-Acid Batteries Using Optimal Control Theory," in *2015 American Control Conference*, (Chicago, IL USA), July 1-3 2015.
17. A. Abdollahi, N. Raghunathan, X. Han, G. V. Avvari, B. Balasingam, K. R. Pattipati, and Y. Bar-Shalom, "Battery Charging Optimization for OCV-Resistance Equivalent Circuit Model," in *2015 American Control Conference*, (Chicago, IL USA), 2015.
18. R. Methekar, V. Ramadesigan, R. D. Braatz, and V. R. Subramanian, "Optimum charging profile for lithium-ion batteries to maximize energy storage and utilization," *ECS Transactions*, **25**(35), 139 (2010).
19. M. Torchio, N. A. Wolff, D. M. Raimondo, L. Magni, U. Krewer, R. B. Gopaluni, J. A. Paulson, and R. D. Braatz, "Real-time Model Predictive Control for the Optimal Charging of a Lithium-ion Battery," in *2015 American Control Conference*, (Chicago, IL USA), 2015.
20. M. Torchio, L. Magni, R. D. Braatz, and D. M. Raimondo, "Design of Piecewise Affine and Linear Time-Varying Model Predictive Control Strategies for Advanced Battery Management Systems," in *Journal of the Electrochemical Society*, **164**(4), A949 (2017).
21. R. Klein, N. Chaturvedi, J. Christensen, J. Ahmed, R. Findeisen, and A. Kojic, "Optimal charging strategies in lithium-ion battery," in *American Control Conference (ACC)*, 2011, pp. 382-387, June 2011.
22. H. Perez, N. Shahmohammadhamedani, and S. Moura, "Enhanced performance of li-ion batteries via modified reference governors and electrochemical models," *IEEE/ASME Transactions on Mechatronics*, **20**, 1511 (2015).
23. X. Hu, S. Li, H. Peng, and F. Sun, "Charging time and loss optimization for LiNMC and LiFePO4 batteries based on equivalent circuit models," *Journal of Power Sources*, **239**(0), 449 (2013).
24. X. Hu, H. E. Perez, and S. J. Moura, "Battery charge control with an electro-thermal-aging coupling," in *ASME 2015 Dynamic Systems and Control Conference*, (Columbus, Ohio, USA), Dynamic Systems and Control Division, ASME, October 2015.
25. H. Perez, X. Hu, S. Dey, and S. Moura, "Optimal Charging of Li-Ion Batteries with Coupled Electro-Thermal-Aging Dynamics," *IEEE Transactions on Vehicular Technology*, vol. **PP**, 1 (2017).
26. H. Perez, X. Hu, and S. Moura, "Optimal charging of batteries via a single particle model with electrolyte and thermal dynamics," in *American Control Conference (ACC)*, 2016, (2016).
27. E. Prada, D. D. Domenico, J. B. Y. Creff, V. Sauvant-Moynot, and F. Huet, "Simplified electrochemical and thermal model of LiFePO4-graphite li-ion batteries for fast charge applications," *Journal of The Electrochemical Society*, **159**(9), A1508 (2012).
28. and P. Kemper and D. Kum, "Extended Single Particle Model of Li-Ion Batteries Towards High Current Applications," in *2013 IEEE Vehicle Power and Propulsion Conference (VPPC)*, pp. 1-6, Oct 2013.
29. X. Han, M. Ouyang, L. Lu, and J. Li, "Simplification of physics-based electrochemical model for lithium ion battery on electric vehicle. Part I: Diffusion simplification and single particle model," *Journal of Power Sources*, **278**, 802 (2015).
30. S. J. Moura, F. B. Argomedo, R. Klein, A. Mirtabatabaei, and M. Krstic, "Battery state estimation for a single particle model with electrolyte dynamics," *IEEE Transactions on Control Systems Technology*, **PP**(99), 1 (2016).
31. ,X. Lin, H. E. Perez, S. Mohan, J. B. Siegel, A. G. Stefanopoulou, Y. Ding, and M. P. Castanier, "A lumped-parameter electro-thermal model for cylindrical batteries," *Journal of Power Sources*, **257**(0), 1 (2014).
32. H. E. Perez, J. B. Siegel, X. Lin, A. G. Stefanopoulou, Y. Ding, and M. P. Castanier, "Parameterization and validation of an integrated electro-thermal cylindrical lfp battery model," in *ASME 2012 5th Annual Dynamic Systems and Control Conference*, (Fort Lauderdale, Florida, USA), pp. 41-50, Dynamic Systems and Control Division, ASME, October 2012.
33. Y. Kim, S. Mohan, J. B. Siegel, A. G. Stefanopoulou, and Y. Ding, "The estimation of temperature distribution in cylindrical battery cells under unknown cooling conditions," *IEEE Transactions on Control Systems Technology*, **22**, 2277 (2014).
34. J. Newman, "Fortran programs for the simulation of electrochemical systems," 2008.
35. J. Marcicki, M. Canova, A. T. Conlisk, and G. Rizzoni, "Design and parametrization analysis of a reduced-order electrochemical model of graphite/lifepo4 cells for soc/soh estimation," *Journal of Power Sources*, **237**, 310 (2013).
36. L. Zhang, C. Lyu, G. Hinds, L. Wang, W. Luo, J. Zheng, and K. Ma, "Parameter sensitivity analysis of cylindrical lifepo4 battery performance using multi-physics modeling," *Journal of The Electrochemical Society*, **161**(5), A762 (2014).
37. M. Safari and C. Delacourt, "Modeling of a commercial graphite/lifepo4 cell," *Journal of The Electrochemical Society*, **158**(5), A562 (2011).
38. J. Strikwerda, *Finite difference schemes and partial differential equations*. Society for Industrial and Applied Mathematics, 2007.
39. M. A. Patterson and A. V. Rao, "GPOPS-II: AMATLAB software for solving multiplephase optimal control problems using hp-adaptive gaussian quadrature collocation methods and sparse nonlinear programming," *ACM Trans. on Mathematical Software (TOMS)*, **41**(1), (2014).
40. I. M. Ross and M. Karpenko, "A review of pseudospectral optimal control: From theory to flight," *Annual Reviews in Control*, **36**(2), 182 (2012).
41. D. Limebeer, G. Perantoni, and A. Rao, "Optimal control of formula one car energy recovery systems," *International Journal of Control*, **87**(10), 2065 (2014). Q1
42. C. L. Darby, W. W. Hager, and A. V. Rao, "An hp-adaptive pseudospectral method for solving optimal control problems," *Optimal Control Applications and Methods*, **32**(4), 476 (2011).
43. D. Garg, W. W. Hager, and A. V. Rao, "Pseudospectral methods for solving infinite-horizon optimal control problems," *Automatica*, **47**(4),829 (2011).

Query

Q1: AU: Please provide a digital object identifier (doi) for Ref(s) 41. For additional information on doi's please select this link: http://www.doi.org/. If a doi is not available, no other information is needed from you.